Journal of Alloys and Compounds 642 (2015) 70–77

Contents lists available at ScienceDirect

Journal of Alloys and Compounds

journal homepage: www.elsevier.com/locate/jalcom

Manganese ferrite prepared using reverse micelle process: Structural and magnetic properties characterization

Mohd. Hashim [a,*], Sagar E. Shirsath [b], S.S. Meena [c], M.L. Mane [d], Shalendra Kumar [e], Pramod Bhatt [c], Ravi Kumar [f], N.K. Prasad [g], S.K. Alla [g], Jyoti Shah [h], R.K. Kotnala [h], K.A. Mohammed [i], Erdoğan Şentürk [j], Alimuddin [a]

[a] Department of Physics, Aligarh Muslim University, Aligarh 202002, India
[b] Spin Device Technology Centre, Department of Engineering, Shinshu University, Nagano 380-8553, Japan
[c] Solid State Physics Division, Bhabha Atomic Research Centre, Mumbai 400085, India
[d] Department of Physics, S.G.R.G. Shinde Mahavidyalaya, Paranda 413502, MS, India
[e] School of Materials Science and Engineering, Changwon National University, Changwon, Gyeongnam 641-773, Republic of Korea
[f] Centre for Material Science Engineering, National Institute of Technology, Hamirpur, HP, India
[g] Deptartment of Metallurgical Engineering, Indian Institute of Technology (Banaras Hindu University), Varanasi 221005, India
[h] National Physical Laboratory (CSIR), Dr. K.S. Krishnan Road, New Delhi 110012, India
[i] Department of Mathematics & Physics Sciences, College of Arts and Sciences, University of Nizwa, Nizwa, Oman
[j] Department of Physics, Sakarya University, Esentepe, 54187 Sakarya, Turkey

ARTICLE INFO

Article history:
Received 9 January 2015
Received in revised form 3 April 2015
Accepted 14 April 2015
Available online 20 April 2015

Keywords:
Nanostructured materials
Chemical synthesis
Magentisation
Mössbauer spectroscopy
X-ray diffraction

ABSTRACT

Reverse microemulsion process was employed to prepare of nanocrystalline Mn^{3+} substituted $MnFe_{2-x}Mn_xO_4$ ferrites. The structural, magnetic and dielectric properties were studied for different concentrations of Mn^{3+}. The structural and microstructural properties were analyzed using X-ray diffraction technique (XRD), transmission electron microscopy (TEM), scanning electron microscopy (SEM) and Fourier transform infrared (FT-IR) spectroscopy techniques. The phase identification of the materials was studied by Rietveld refined XRD patterns which reveals single phase with cubic symmetry for the samples. The lattice parameters were ranged in between 8.369 and 8.379 Å and do not show any significant change with the substitution of Mn^{3+}. The average particles size was found to be around 11 ± 3 nm. Magnetization results obtained from the vibrating sample magnetometer (VSM) confirm that the substitution of Mn^{3+} in $MnFe_2O_4$ ferrite caused an increase in the saturation magnetization and coercivity. The dependence of Mössbauer parameters on Mn^{3+} substitution has been analyzed. Magnetic behavior of the samples were also studied at field cooled (FC) and zero field cooled (ZFC) mode. The dependence of Mössbauer parameters on Mn^{3+} substitution was also analyzed. All the magnetic characterization shows that Mn^{3+} substitution enhance the magnetic behavior of $MnFe_2O_4$ ferrite nanoparticles.

1. Introduction

The unique and novel size dependent chemical and physical properties articulated by metal and semiconductor nanocrystals have commenced the present extensive assortment of rigorous investigation on nano materials [1,2]. Recently, extreme zests have been broadcast into restraining the shape of nano materials and also into understanding the correlations between material properties and its shape. The shape of nano materials can be as vital as the size in determining the uniqueness and novelty of material properties. Moreover, a large part of the societal impact by nano materials surely will be realized in a variety of devices consisting of nano material components. Manganese ferrites belong to a family of soft ferrite materials characterized by high magnetic permeability and low losses. Furthermore, it is also ascribed that Mn ferrites are of inverse spinel structure because 80% of Mn ions occupy tetrahedral site (A-site), which is surrounded by four O^{2-} ions, and the left 20% of Mn ions occupy octahedral site (B-site), which is surrounded by six O^{2-} ions. The cation distribution for Mn ferrites can be represented by $(Mn^{2+}_{0.8}Fe^{3+}_{0.2})^A\ [Mn^{3+}_{0.2}Fe^{2+}_{0.2}Fe^{3+}_{1.6}]^B\ O_4$ [3,4]. These materials are predominantly consumed in numerous applications such as microwave devices, computer memory chips, magnetic recording media, radio frequency coil fabrication, transformer cores, rod antennas and many branches of telecommunication and electronic engineering [5–8]. Congregation of nano-components is a key itinerary

* Corresponding author. Tel.: +91 9359380185.
E-mail address: md.hashim09@gmail.com (Mohd. Hashim).

http://dx.doi.org/10.1016/j.jallcom.2015.04.085
0925-8388/

in building devices, and the outline of nano-building blocks and associated properties will be decisive for the congress and gadget designs. Shape-controlled synthesis of nanocrystals certainly is an experimental challenge. Successes in shape control of nanocrystals have been reported in the syntheses of metals and semiconductors. Clearly, it is desirable to develop strategies for shape controlled syntheses of complex metal oxides possessing rich properties, especially the electric and magnetic characteristics. The most operable techniques of synthesis of nano materials include formation through a chimie douce solution chemistry methodology, a sol–gel processing mechanism, the use of microemulsions, the utilization of hydrothermal and solvothermal methods, the kinetic control of growth through the use of capping reagents, the application of template-inspired methodologies, and lastly, bio-mimetic synthesis. The microemulsion technique promises to be one of the adaptable research process which enables to manage the particle properties such as mechanisms of particle size control, geometry, morphology, homogeneity and surface area. The uses and applications of microemulsions are copious in chemical and biological fields. The nanoparticles not only are of fundamental scientific attention, but also have resulted in important technological applications, such as catalysts, high-performance ceramic materials, microelectronic devices, high-density magnetic recording and drug delivery.

In the present research work the microstructures, morphology, magnetic and electrical properties of Mn^{3+} substituted $MnFe_2O_4$ ferrite nanoparticles were studied by means of various experimental techniques. The samples were synthesized with a chemical formula $Mn^{2+}Fe^{3+}_{2-x}Mn^{3+}{}_xO_4$ where Mn^{3+} is substituted for Fe^{3+} from $x = 0.0$ to $x = 1.0$ in steps of 0.25. The XRD results infer the single phase nature of $MnFe_{2-x}Mn_xO_4$ ferrite nanoparticles. DC magnetization results show increase in saturation of magnetization and coercive field with increase in the Mn content, Mossbauer spectroscopy results indicate that magnetic interactions increases with Mn doping.

2. Experimental

Weighted amounts of all analytical grade reagents were used as received without further purification in order to obtain homogeneous morphology and stoichiometry of $MnFe_{2-x}Mn_xO_4$ nanoparticles by reverse microemulsion technique. Metal nitrates of respective cations were used as metal precursors. The Preparation procedure of $MnFe_{2-x}Mn_xO_4$ ferrite nanoparticles by the reverse microemulsion technique is displayed in Fig. 1, with cyclohexane as oil, cetyl-tri-methyl-ammonium bromide (CTAB) as surfactant, isoamylalcohol as the co-surfactant phase. Micro-emulsions were prepared by adding to 10.20 g of CTAB, 12.81 ml of isoamylalcohol and 30.48 ml of cyclohexane with 5.5 wt% of an aqueous solution of the reactants, corresponding to the desired value of Water/[CTAB] ratio being equal to 10.12. The emulsions were sonicated until clear solutions formed. In order to synthesize $MnFe_{2-x}Mn_xO_4$ ferrite, two microemulsions were prepared: one containing the metal salts prepared by mixing stoichiometric amounts of ferrite and manganese nitrates. Second reverse micro-emulsion solution was prepared with 0.1 M aqueous solution of NaOH as water phase under similar conditions. The solutions were mixed quickly with vigorous stirring at constant temperature (80 °C) and pH of the resulting solution was maintained at 9. The resulting solution was continuously stirred for another 2 h in order to complete the reaction. An equal volume of acetone and isopropanol was added to the resulting solution and centrifuged to separate the solid product. The product was washed with water and acetone and dried in an air oven at 100 °C for 36 h. After the powders formation the samples were annealed at 700 °C for 4 h, the mixtures were pressed into pellet form by using a hydraulic press at 8 ton/cm^2. These samples were used in powder form for the X-ray diffraction (XRD), transmission electron microscopy (TEM), scanning electron microscopy (SEM), Fourier transform infrared spectroscopy (FTIR), vibrating sample magnetometer (VSM), SQUID magnetometer (for isothermal DC magnetization measurements) and the Mössbauer spectroscopy experiments. The sintered pellets were used to measure the electric and dielectric behavior of these samples.

3. Results and discussion

3.1. Structural study

The Rietveld refined XRD patterns of $MnFe_{2-x}Mn_xO_4$ at different concentrations of Mn^{3+} is illustrated in Fig. 2. The matching of the standard *d* values with the observed planes in the diffraction patterns confirms the formation of a cubic spinel structure. The main reflections from planes (220), (311), (400), (422), (333), (511) and (440) characterizing spinel ferrites are clearly observed without any trace of detectable impurity. The XRD of the prepared sample ($MnFe_{2-x}Mn_xO_4$) seems to be different from one another, mainly due to (i) the concentration of Mn cations, (ii) the difference in the crystal size of the obtained powder, and (iii) relative change in lattice constant.

The lattice parameters were calculated from the XRD patterns data and are presented in Fig. 3. The lattice constant is influenced by the cationic stoichiometry. The lattice parameter values which were calculated using Bragg's Law do not showed any significant trend with the substitution of Mn^{3+}. This may be due to the similar size of the ionic radii of Fe^{3+} and Mn^{3+} ions. The ionic radii of Fe^{3+} and Mn^{3+} are 0.67 and 0.645 Å respectively. The average particle size was calculated from the (311) diffraction peak of the XRD profiles using the well-known Debye Scherer equation. From the calculation, the particle size tends to decrease with from 28 to 23 nm with increase in Mn^{3+} concentration. Typical TEM and

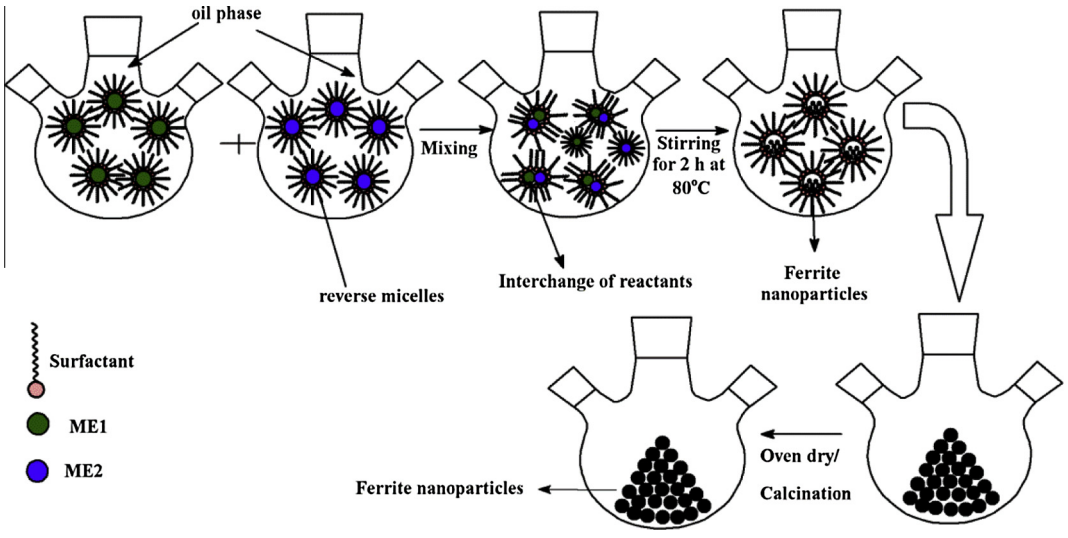

Fig. 1. Schematic of the preparation of $Mn^{3+}{}_xMn^{2+}Fe_{2-x}O_4$ ferrite synthesized by reverse microemulsion technique.

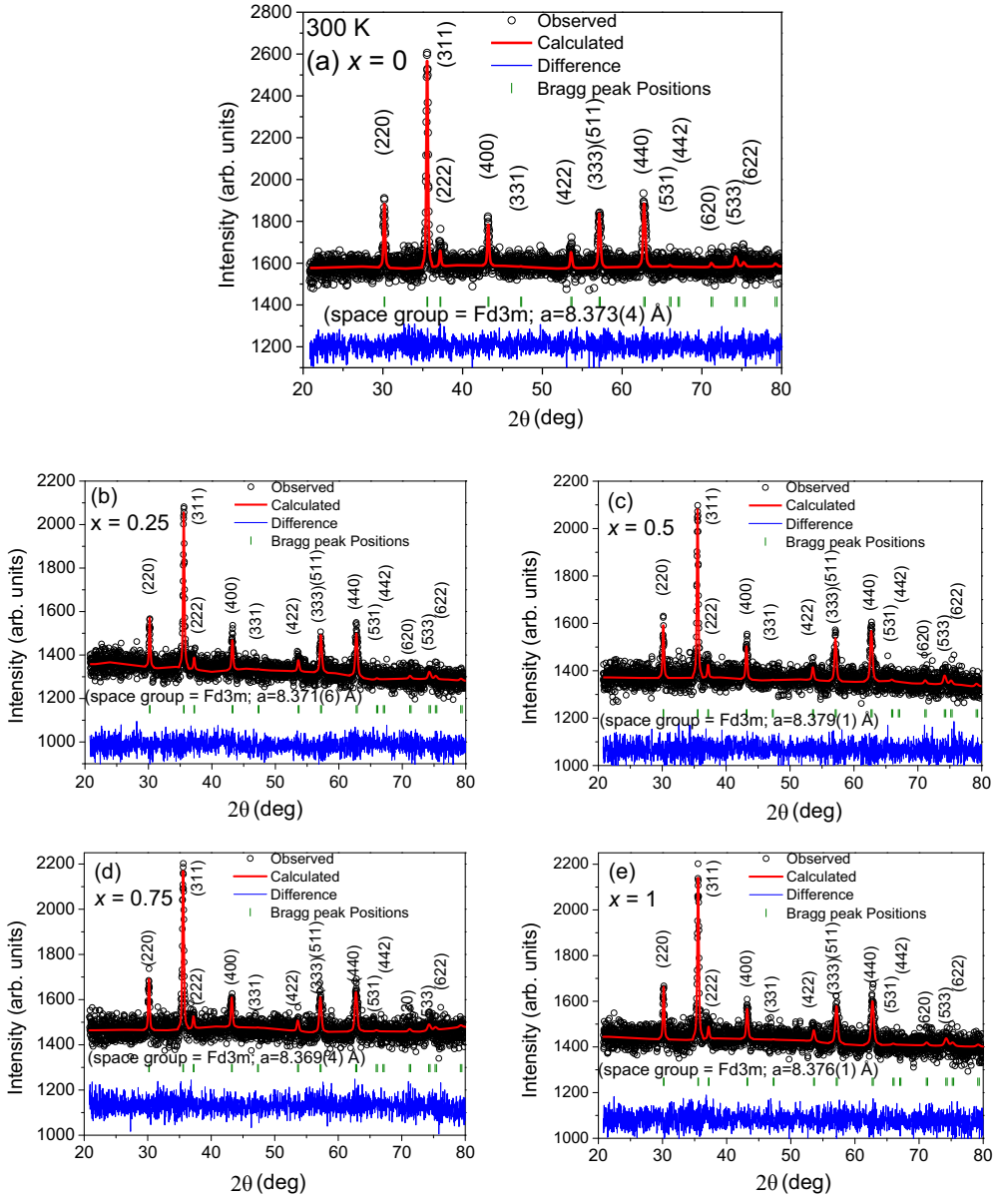

Fig. 2. Rietveld refined X-ray diffraction patterns of $Mn^{3+}_{x}Mn^{2+}Fe_{2-x}O_4$ for (a) $x = 0.0$, (b) $x = 0.25$, (c) $x = 0.5$, (d) $x = 0.75$ and (e) $x = 1.0$.

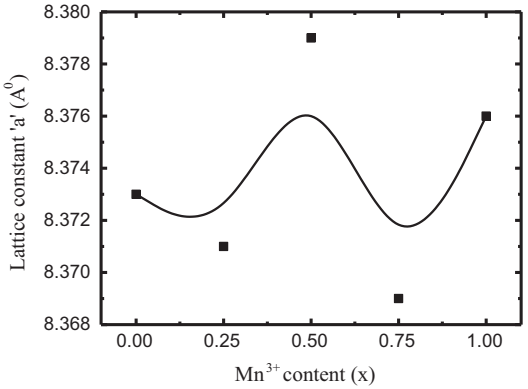

Fig. 3. Variation of lattice constant (a) with Mn^{3+} substitution in $Mn^{3+}_{x}Mn^{2+}Fe_{2-x}O_4$.

SEM micrographs of the synthesized Mn^{3+} substituted Mn-ferrite nanoparticles showed (Figs. 4 and 5) that most of the ferrite particles were fine, homogeneous with narrow particle distributions. The typical TEM micrograph for $Mn^{3+}_{x}Mn^{2+}Fe_{2-x}O_4$ for composition $x = 0.5$ is shown in Fig. 4(a). Most of the particles are individual however some of them are agglomerated. The average particles size was found to be in the range of 4–22 nm. The size distribution of the particles was also estimated by counting 50 nanoparticles from random view field of TEM micrograph using Image J software and it is shown in Fig. 4(b). It suggests that the average particles size was around 11 ± 3 nm. The SAD pattern of the sample suggests that it was essentially a F.C.C. crystal structure which confirms our XRD finding. The SEM micrographs of the $Mn^{3+}_{x}Mn^{2+}Fe_{2-x}O_4$ samples for (a) $x = 0.0$, (b) $x = 0.25$, (c) $x = 0.5$ and (d) $x = 1.0$ are shown in Fig. 5. Particles are almost agglomerated. From the contrast of the particles (due to charging) we may say that the samples are essentially oxide phase. It can further be assumed that there is no other phase except $Mn^{3+}_{x}Mn^{2+}Fe_{2-x}O_4$ phase, as no particles with different contrast were observed.

Fig. 6 shows the infrared spectra of all the samples under investigation. The vibronic studies using infrared radiation are a good

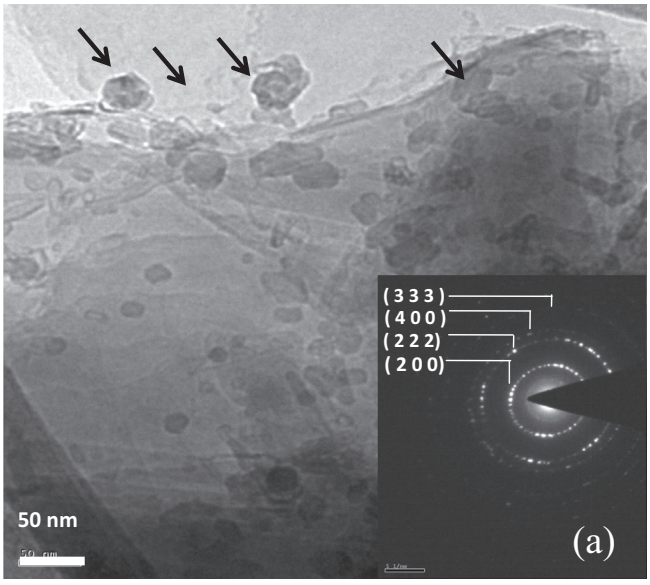

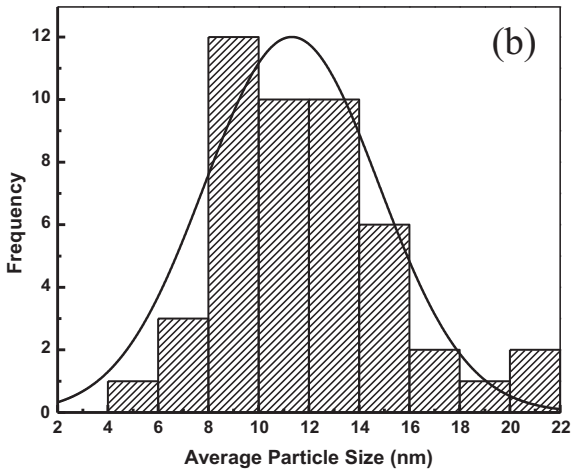

Fig. 4. (a) TEM micrograph of $Mn^{3+}_{x}Mn^{2+}Fe_{2-x}O_4$ for composition $x = 0.5$ (Bar = 50 nm). The inset shows selective area electron diffraction (SAD) pattern. Arrows indicate agglomerated particles. (b) Particles size distribution of the same sample.

fingerprint for the local chemical bonds. According to the Waldron [9], the ferrites can be considered continuously bonded crystals, meaning that the atoms are bounded to all the nearest neighbors by equivalent forces. In spinel ferrites, the metal ions are located into two sub-lattices namely tetrahedral (A-site) and octahedral (B-site) according to the geometrical configuration of the oxygen nearest neighbors. The appearance of low frequency bands in the range of 400–600 cm^{-1}, ν_2 and ν_1 respectively are assigned to the intrinsic vibration of tetrahedral and octahedral complexes [9]. The absorption bands observed within this range is an indication of the formation of single phase spinel structure. In the present study ν_2 is observed in the wavenumber range of 572 ($x = 0.0$)–586 ($x = 1.0$) cm^{-1} and it shows increasing trend with increase in Mn^{3+} concentration. On the other hand ν_1 slightly increased from 465 ($x = 0.0$) to 472 ($x = 1.0$) cm^{-1}. This variation in ν_2 and ν_1 giving an evidence that the Mn^{3+} ions affect the cation distribution of $MnFe_{2-x}Mn_xO_4$. Moreover, Mn^{3+} occupy the octahedral site more as compared to that of tetrahedral site. Further, the difference in band positions is attributed to the difference in the Fe^{3+} to O^{2-} distances for tetrahedral and octahedral complexes.

3.2. Magnetic properties

The magnetizations vs. field curves of the Mn-ferrite samples measured at room temperature using VSM are shown in Fig. 7. The hysteresis loops of the samples displayed narrow hysteretic loops of soft ferromagnetic materials and shows obvious differences as manganese content was changed. It is clear from Fig. 8 that saturation magnetization (M_S) increased from 16 to 30 emu/g whereas coercivity (H_C) increased from 115 to 223 Oe. The increase in M_S is quite interesting even though the magnetic moment of Mn^{3+} is lower (=4.97 μ_B) compared to that of Fe^{3+} (=5 μ_B). It is our hypothesis that the change in the ionic distribution causes enhancement in saturation magnetization. It is known fact that in the spinel ferrite saturation magnetization is depend on the exchange interaction between the A and B site i.e. A–B exchange interaction. Mn^{3+} ions assumed to occupy the B site replacing Fe^{3+} ions. The increased concentration of Mn^{3+} ions at B site might have enhanced the exchange interaction between Mn^{2+} ions of A site and Mn^{3+} ions of B site.

The Mössbauer spectra of the presently investigated system are shown in Fig. 9. It is observed from Fig. 9 that the lines of the B-site patterns are broadened and certain overlapping appears, so the A and B-site pattern is fitted into several components to obtain the A and B-site subpatterns. The appearance of several components is due to the different cations at the A and B-site. In our study, the A and B-site is occupied by Fe^{3+}, Mn^{2+} and Mn^{3+}, though the Fe^{3+} and Mn^{3+} prefer octahedral B-site. The variation in Mössbauer parameters with Mn^{3+} substitution; such as hyperfine field (H_{hf}), isomer shift (δ), quadrupole splitting (Δ), linewidth (Γ) and relative areas (R_A) can be determined from the above mentioned sub patterns. The values of H_{hf}, δ, Δ, Γ and R_A are tabulated in Table 1. On the basis of δ and H_{hf} values, it can be stated that the sextet D is due to the tetrahedral site and the other patterns {Doublets (A and B), sextet A, sextet B and sextet C} are due to octahedral site. It can be observed from Table 1 that the isomer shift value for octahedral sites is more than that for tetrahedral sites. In cubic spinel ferrites, the bond separation Fe^{3+}–O^{2-} is larger for octahedral sites when compared to that for tetrahedral sites. Due to this, overlapping of orbital of Fe^{3+} ions is small at B-sites and thus a larger isomer shift at B-sites was expected [10–12]. The observed variation of isomer shift shows an insignificant change with increasing substitution of Mn^{3+} ions. It implies that the s-electron charge density of Fe^{3+} ions is not much influenced by increased Mn^{3+} substitution. The variation of quadrupole splitting for hyperfine spectra of all the samples are found to be negligibly small (except doublets, Δ is nearly zero for all sextets) and attributed to the fact that overall cubic symmetry is maintained between Fe^{3+} ions and their surroundings with Mn^{2+} and the substituted Mn^{3+} ions. It is observed that hyperfine field increased with increasing Mn^{3+} substitution up to $x = 0.75$ and this can be qualitatively explained using Neel's super-exchange interactions. As both A and B sites are occupied by Fe^{3+} ions, so the interaction of Fe^{3+} is possible with Mn^{2+} and Mn^{3+} ions. In the present series Fe^{3+} ions are replaced by Mn^{3+} ions with a magnetic moment. This results increase of magnetic linkages in Fe^{3+}_A—O—Fe^{3+}_B, Fe^{3+}_A—O—Mn^{2+}_A, Fe^{3+}_A—O—Mn^{2+}_B and Mn^{2+}_A—O—Mn^{3+}_B. Hence $MnFe_{2-x}Mn_xO_4$ experiences an increase in the magnetic field at A and B sites and hyperfine magnetic field is also expected to increase with increase of Mn^{3+} concentration. Usually the saturation magnetization is proportional to the hyperfine field which agrees well with hysteresis measurements [13,14].

Fig. 10 shows the variation of magnetization (M) as a function of temperature (T) in the range 50–350 K in the zero field cooling (ZFC) and field cooling (FC) modes for typical samples $x = 0.0$, 0.50 and 1.0. The ZFC curves shows peak at ~175 K for $x = 0.0$

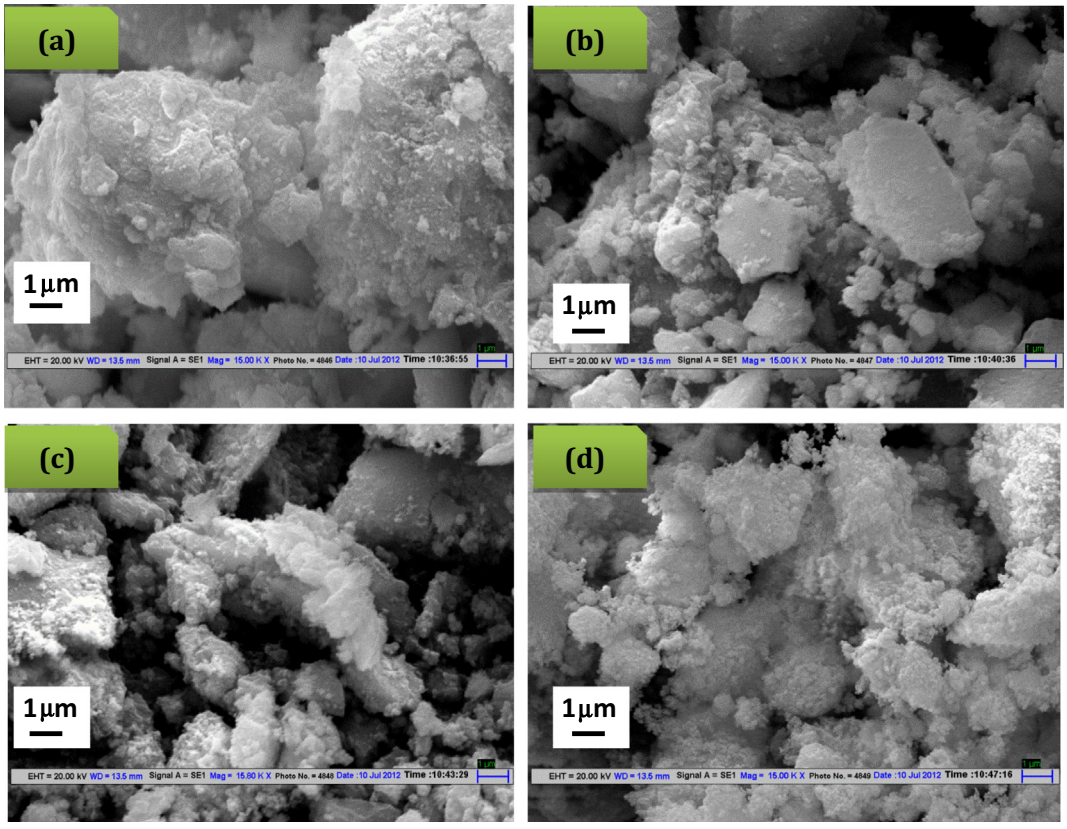

Fig. 5. Scanning electron microscopy (SEM) images of $Mn^{3+}_{x}Mn^{2+}Fe_{2-x}O_4$ for (a) $x = 0.0$, (b) $x = 0.25$, (c) $x = 0.5$ and (d) $x = 1.0$.

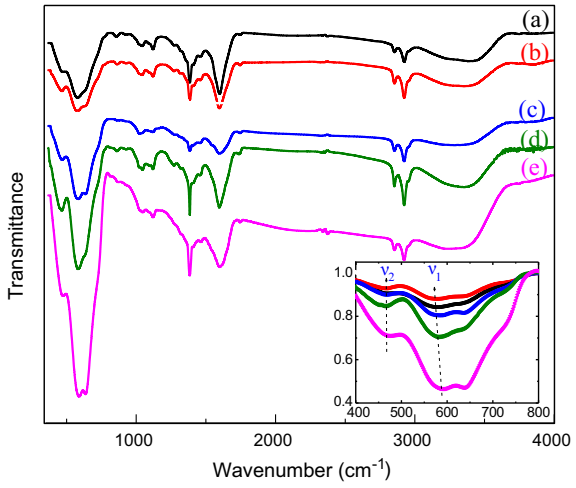

Fig. 6. FTIR spectra of $Mn^{3+}_{x}Mn^{2+}Fe_{2-x}O_4$ for (a) $x = 0.0$, (b) $x = 0.25$, (c) $x = 0.5$, (d) $x = 0.75$ and (e) $x = 1.0$.

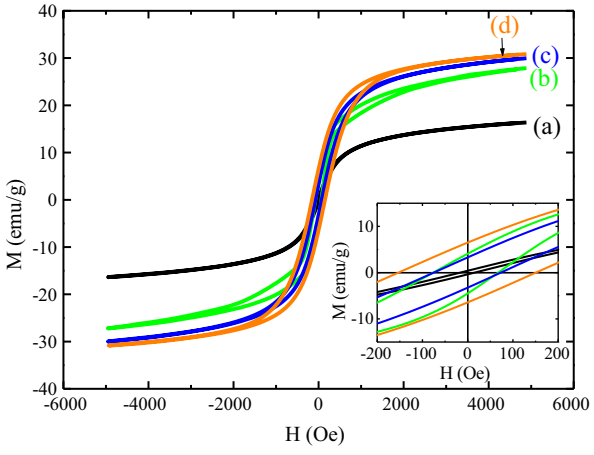

Fig. 7. Variation of magnetization with applied magnetic field of $Mn^{3+}_{x}Mn^{2+}Fe_{2-x}O_4$ for (a) $x = 0.0$, (b) $x = 0.25$, (c) $x = 0.5$ and (d) $x = 1.0$ at room temperature. *Inset shows the variation of magnetization at low applied field.*

which indicates it's blocking temperature (T_B) and similarly the T_B was found to be near 200 and 280 K for $x = 0.5$ and 1.0 respectively.

3.3. Dielectric properties

The dielectric properties of the samples have been studied as a function of concentration at different frequencies. Permittivity in an AC electric field is defined as complex relative permittivity ε, given by

$$\varepsilon = \sigma - j\varepsilon'' \quad (1)$$

The value of dielectric constant (ε') has been calculated using the relation:

$$\varepsilon' = \frac{C_p \times d}{\varepsilon_0 A} \quad (2)$$

where C_p is the capacitance of parallel pellet in F, d is the thickness of pellet in cm, A is the cross-sectional area of the flat surfaces of the pellet in cm^2 and ε_0 is the free space permittivity. Fig. 11 shows that the room temperature dielectric constant is observed to decrease with the increase in Mn^{3+} ion concentration. The dielectric constant of any material, in general, is due to dipolar, electronic, ionic and

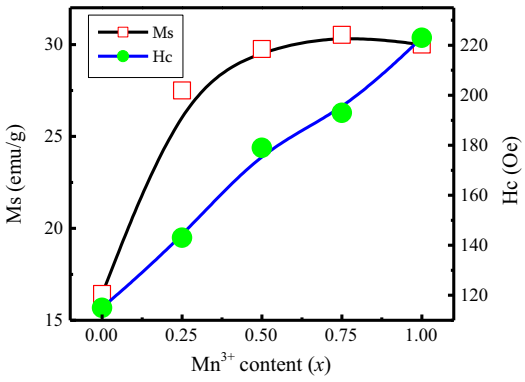

Fig. 8. Variation in saturation magnetization (M_S) and coercivity (H_C) with Mn^{3+} substitution of $Mn^{3+}_xMn^{2+}_xFe_{2-x}O_4$.

interfacial polarizations. At low frequencies, dipolar and interfacial polarizations are known to play dominant role and both these polarizations are frequency dependent [15,16]. The high values of dielectric constant at lower frequencies come from the combined effect of interfacial and dipolar polarizations. At higher frequencies, electronic and ionic polarizations are the main contributors. A barrier-layer structure with semiconducting areas encircled by insulating layers can be used to explain the variation of dielectric constant at low frequency. This behavior is considered by the space charge polarization arising from differences between the conductivity of the various phases present. Ferrites structurally form cubic close packed oxygen lattices with the cations at the octahedral (B) and the tetrahedral (A) sites. The distance between two cations at B sites is smaller than the distance between a cation at B site and another cation at an A site. Compared to B–B hopping, the A–B hopping probability is small and hopping between A and A sites does not exist as Fe^{3+} ions exist at A site and any Fe^{2+} ion formed during preparation occupy only the B sites. Therefore, hopping of electrons between Fe^{2+} and Fe^{3+} ions at B sites is the main mode of conduction [17]. The electrons, by hopping, reach the grain boundary and due to its higher resistivity, the electrons get piled up, thereby producing space charge polarization. In the low frequency region electron hopping occurs between Fe^{3+} and Fe^{2+} on the octahedral sites. The electrons arrive at the grain boundary through hopping and are piled up at the grain boundaries, which grades in the interfacial polarization. However, as the frequency is increased, the probability

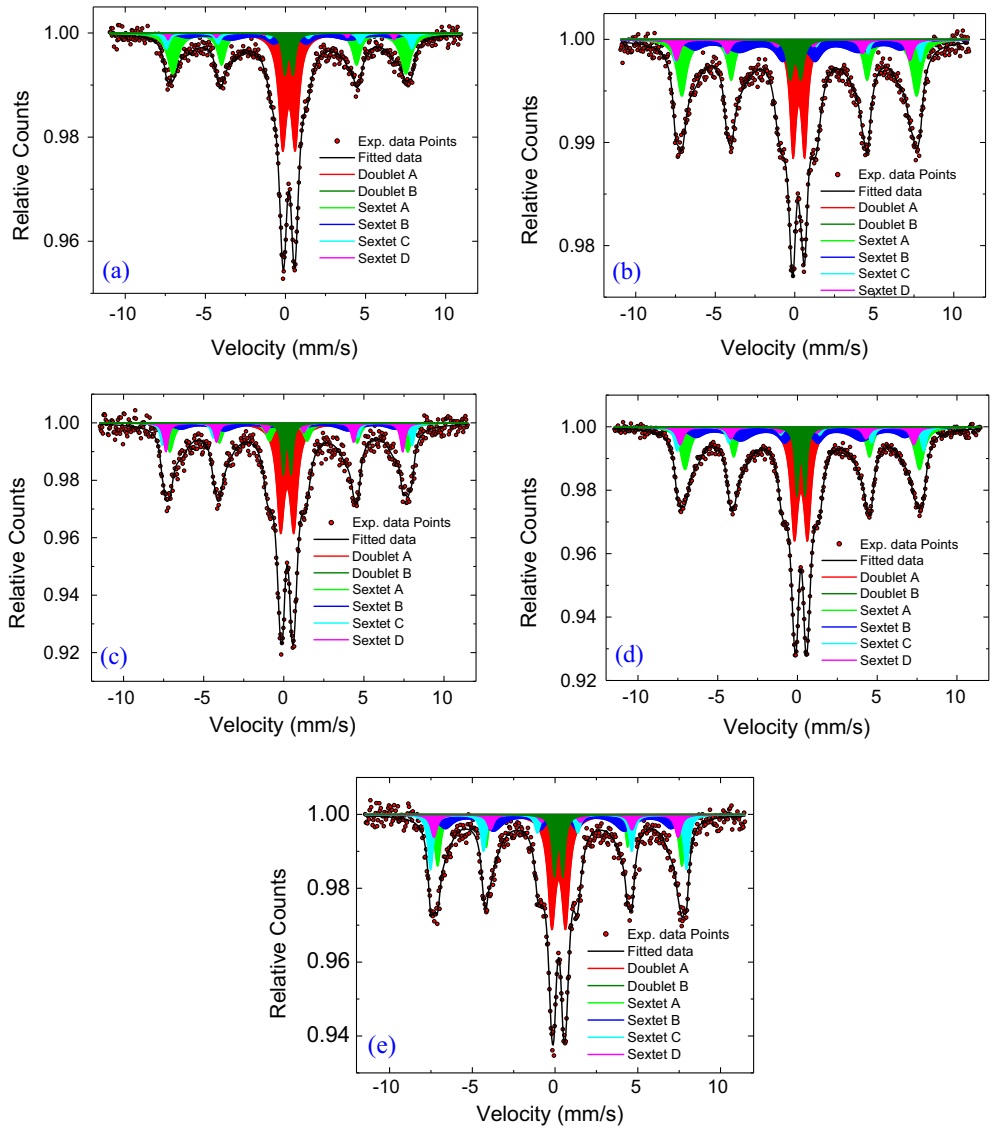

Fig. 9. Room temperature (300 K) Mössbauer spectra of $Mn^{3+}_xMn^{2+}Fe_{2-x}O_4$ for (a) $x = 0.0$, (b) $x = 0.25$, (c) $x = 0.5$, (d) $x = 0.75$ and (e) $x = 1.0$.

Table 1
The hyperfine field values (H_{hf}), isomer shift (δ), quadrupole splitting (Δ), line width (Γ), relative areas (R_A) in percentage of Fe sites for $Mn^{3+}_xMn^{2+}Fe_{2-x}O_4$ (x = 0.0–1.0) and fitting quality factor (χ^2) derived from Mössbauer spectra recorded at room temperature. Isomer shift values are relative to α-Fe metal foil (δ = 0.0 mm/s). *Square bracket denotes the estimated error.*

Mn^{3+} (x)	Iron sites	R_A (%)	Γ (mm/s) [±0.06]	δ (mm/s) [±0.02]	Δ (mm/s) [±0.02]	H_{hf} (Tesla) [±0.16]	χ^2
0.0	Doublet A	24.1	0.577	0.329	0.783	–	1.03264
	Doublet B	3.3	0.353	0.327	0.511	–	
	Sextet A	23.4	0.318	0.345	0.018	45.11	
	Sextet B	39.7	1.029	0.403	0.009	39.84	
	Sextet C	8.3	0.434	0.338	0.008	47.48	
	Sextet D	1.2	0.256	−0.139	−0.057	43.72	
0.25	Doublet A	9.8	0.473	0.369	0.724	–	1.07529
	Doublet B	3.1	0.458	0.16	0.665	–	
	Sextet A	29.4	0.511	0.39	0.003	45.77	
	Sextet B	45.1	1.021	0.334	−0.078	40.15	
	Sextet C	4.3	0.348	0.278	0.053	47.8	
	Sextet D	8.3	0.491	0.07	−0.116	45.5	
0.50	Doublet A	18.9	0.574	0.326	0.825	–	0.93775
	Doublet B	2.2	0.282	0.326	0.489	–	
	Sextet A	24.5	0.578	0.411	0.032	46.04	
	Sextet B	39.0	1.423	0.324	0.086	41.42	
	Sextet C	6.9	0.365	0.280	0.105	48.12	
	Sextet D	8.4	0.356	0.170	−0.047	45.72	
0.75	Doublet A	15.6	0.554	0.331	0.8179	–	1.02966
	Doublet B	2.8	0.299	0.336	0.507	–	
	Sextet A	22.3	0.441	0.392	0.042	46.57	
	Sextet B	41.5	0.901	0.329	−0.045	42.67	
	Sextet C	8.8	0.432	0.294	0.009	48.14	
	Sextet D	9.0	0.507	0.13	−0.093	45.75	
1.0	Doublet A	17.3	0.557	0.332	0.830	–	0.89444
	Doublet B	3.3	0.327	0.326	0.511	–	
	Sextet A	15.5	0.378	0.312	0.169	45.77	
	Sextet B	35.7	0.729	0.323	−0.038	42.31	
	Sextet C	18.1	0.393	0.294	0.052	47.95	
	Sextet D	10.1	0.455	0.328	−0.315	45.74	

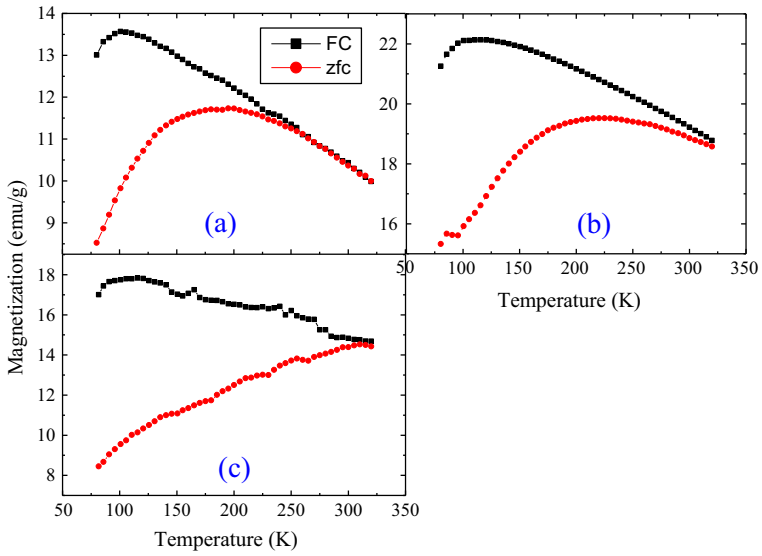

Fig. 10. Variation infield cooled (FC) and zero field cooled (ZFC) of $Mn^{3+}_xMn^{2+}Fe_{2-x}O_4$ for (a) x = 0.0, (b) x = 0.5 and (c) x = 1.0.

of electrons reaching the grain boundary decreases, which results in a decrease in the interfacial polarization [18]. Therefore, the dielectric constant decreases with increasing frequency. Also as reported by several researchers, hopping of electrons between Fe^{2+} and Fe^{3+} (n-type semiconductor) and hopping of holes between Mn^{3+} and Mn^{2+} (p-type semiconductor) are responsible for the conduction process [3]. Accordingly the ferrite is assumed to be made up of well-conducting grains separated by poor conducting layers or grain boundaries. The transport of charge carrier creates the space charge polarization and these charge carriers are stopped at a potential barrier, which is possibly the grain boundary. This can also be understood by a mechanism similar to conduction mechanism. It is seen from the figure that the dielectric constant shows the maximum values for the composition x = 0.0. It can be explained on the

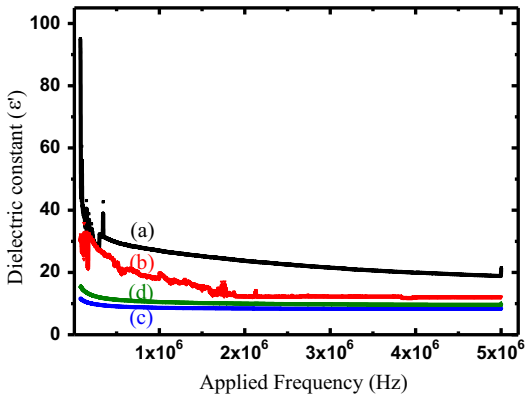

Fig. 11. Variation of dielectric constant (ε') with applied frequency of $Mn^{3+}_{x}Mn^{2+}Fe_{2-x}O_4$ for (a) $x = 0.0$, (b) $x = 0.25$, (c) $x = 0.5$ and (d) $x = 1.0$ at room temperature.

basis that as the Mn^{3+} ions doped in Mn ferrite prefer the B-site. The increase in number of Mn^{3+} ions at octahedral sites decreases the rate of hopping which in turn, decreases the dielectric constant.

4. Conclusions

Mn^{3+} substituted $MnFe_2O_4$ ferrite were successfully synthesized by the reverse microemulsion technique. Structural analysis with Rietveld refined XRD reveals that the system confirms the formation of single phase cubic spinel structure. Lattice constant do not show any significant change with Mn^{3+} substitution due to the comparable ionic radii of Mn^{3+} ions with Fe^{3+} ions. Selective area electron diffraction (SAD) pattern also infers crystalline single phase of cubic structure. From the TEM study, it can be said that particles had dimension in the range of 4–22 nm but most of them were around 11 ± 3 nm. Infrared spectra shows two prominent bands corresponding to spinel ferrite phase. Magnetic studies suggest that the samples were ferromagnetic at room temperature. The Mössbauer measurements showed well resolved magnetic spectra for the tetrahedral and octahedral sites. The hyperfine magnetic field at both the sub lattices increases with the introduction of increasing Mn^{3+} ions by strengthening the exchange interactions. The dielectric constant and ac conductivity increased with Mn^{3+} substitution as Mn^{3+} ion substitutes for Fe^{3+} ions leading to decrease of the hopping rate of electrons between $Fe^{3+} + Mn^{2+} \leftrightarrow Fe^{2+} + Mn^{3+}$. The frequency dependence of dielectric constant and ac conductivity can be understood through Maxwell–Wagner type interfacial polarization.

Acknowledgments

Shalendra Kumar is thankful for the financial assistant support from the Basic Science Research Program through the National Research Foundation of Korea (NRF) funded by the Ministry of Education, Science and Technology (MEST; 2012-0009457) and by the Priority Research Centers Program through the National Research Foundation of Korea (NRF) funded by the Ministry of Education, Science and Technology (MEST; 2012-045424).

References

[1] S. Maensiri, C. Masingboon, B. Boonchom, S.S. Eraphin, Scripta Mater. 56 (2007) 797.
[2] Alex Goldman, Modern Ferrite Technology, second ed., Springer, New York, 2006.
[3] R.H. Kadam, A.R. Biradar, M.L. Mane, Sagar E. Shirsath, J. Appl. Phys. 112 (2012) 043902.
[4] Sagar E. Shirsath, B.G. Toksha, R.H. Kadam, S.M. Patange, D.R. Mane, Ganesh S. Jangam, Ali Ghasemi, J. Phys. Chem. Solids 71 (2010) 1669.
[5] Q.M. Wei, Jian-biao Li, Yong-jun Chen, Yong-sheng Han, Mater. Charact. 47 (2001) 247.
[6] J.A.T. Taylor, S.T. Reczek, A. Rosen, Soft ferrite processing, Am. Ceram. Soc. Bull. 74 (4) (1995) 91–94.
[7] M. Rozman, M. Drofenik, J. Am. Ceram. Soc. 81 (7) (1998) 1757–1764.
[8] S.H. Chen, S.C. Chang, L.N. Lin, J. Magn. Magn. Mater. 209 (2000) 193–196.
[9] R.D. Waldron, Phys. Rev. 99 (1955) 1727.
[10] S.S. Shinde, Sher Singh Meena, S.M. Yusuf, K.Y. Rajpure, J. Phys. Chem. C 115 (2011) 3731–3736.
[11] Mohd. Hashim, Alimuddin, Sagar E. Shirsath, S.S. Meena, R.K. Kotnala, Ameena Parveen, Aashis S. Roy, Shalendra Kumar, Pramod Bhatt, Ravi Kumar, J. Magn. Magn. Mater. 341 (2013) 148–157.
[12] A. Lakshman, P.S.V. Subba Rao, K.H. Rao, Mater. Lett. 60 (2006) 7.
[13] S.M. Patange, Sagar E. Shirsath, B.G. Toksha, S.S. Jadhav, K.M. Jadhav, J. Appl. Phys. 106 (2009) 023914.
[14] Mohd. Hashim, Alimuddin, Shalendra Kumar, Sagar E. Shirsath, R.K. Kotnala, Jyoti Shah, Ravi Kumar, Mater. Chem. Phys. 139 (2013) 364–374.
[15] C.G. Koops, On the dispersion of resistivity and dielectric constant of some semiconductors at audio frequencies, Phys. Rev. 83 (1951) 121–124.
[16] J.C. Maxwell, Electricity and Magnetism, vol. 2, Oxford University Press, New York, 1973.
[17] Sagar E. Shirsath, Santosh S. Jadhav, B.G. Toksha, S.M. Patange, K.M. Jadhav, Scripta Mater. 64 (2011) 773–776.
[18] I.T. Rabinkin, Z.I. Novikova, Ferrites, Izv Acad. Nauk USSR Minsk (1960).